Safe Autonomous Guidance Under Uncertainty via Sequential Covariance Steering for Small-body Proximity Operations

Luca Frassinella[(1)], Kenshiro Oguri[(2)], Francesco Topputo[(1)]

[(1)] *Department of Aerospace Science and Technology, Politecnico di Milano*
Via La Masa 34, 20156, Milan, Italy
luca.frassinella@mail.polimi.it, francesco.topputo@polimi.it

[(2)] *School of Aeronautics and Astronautics, Purdue University*
West Lafayette, Indiana, USA, 47907
koguri@purdue.edu

Abstract **– This paper presents a chance-constrained covariance steering framework for safe autonomous proximity operations around small bodies under navigation uncertainty, maneuver execution errors, and unmodeled accelerations. The method combines linear covariance steering with sequential convex programming to jointly design nominal transfers and affine trajectory correction policies, while satisfying probabilistic and passive-safety constraints. Passive safety is guaranteed in off-nominal scenarios by requiring ballistic trajectories after a missed-thrust event (MTE) to remain outside a keep-out zone with prescribed probability over a continuous-time safety horizon. Two objective formulations are compared: the first minimizes the statistical fuel cost through the ΔV_{99} metric, while the second minimizes a convex bound on nonlinear dynamical effects using higher-order dynamical information from State Transition Tensors (STTs). The framework is applied to representative transfers between Periodic and Resonant Terminator Orbits around asteroid (99942) Apophis and validated through nonlinear Monte Carlo simulations. Results show that both formulations satisfy the passive-safety requirements, while the minimum nonlinearity cost improves coherence between linear covariance predictions and nonlinear sample statistics in highly nonlinear regimes, with only a limited increase in fuel consumption.**

I. Introduction

Close-proximity operations around small bodies are influenced by highly nonlinear dynamics and uncertainties that can perturb the spacecraft's nominal trajectory. Autonomy and robustness in these regimes are especially crucial due to the long ground communication delays and the fast dynamics. In this context, several works have previously addressed autonomous small-body exploration, including autonomous mission architectures and navigation strategies [1–3], as well as robust hovering and close-proximity guidance under uncertainty [4–6]. Trajectory design under uncertainty around small bodies has been investigated through terminator-orbit transfers minimizing covariance and energy [7], chance-constrained robust guidance [8], stochastic primer-vector theory [9], and onboard trajectory refinement for autonomous mapping campaigns [10].

Stochastic optimal control and chance-constrained covariance steering have emerged in the literature as promising tools for robust trajectory optimization under operational uncertainties. Chance-constrained control enables safety requirements to be imposed probabilistically, which is particularly suitable when the uncertainty sources are modeled through unbounded distributions, e.g. Gaussians [11, 12]. Recent works have combined covariance steering with sequential convex programming (SCP) for robust trajectory design in nonlinear astrodynamics environments, an approach referred to as *sequential covariance steering*, including applications to cislunar transfers and interplanetary mission design [13–15]. However, its application to small-body proximity operations remains largely unexplored.

This paper designs safe and autonomous science-orbit transfers around small bodies by applying sequential covariance steering, simultaneously designing robust nominal trajectories and feedback control policies, to probabilistically guarantee safety under navigation uncertainty, maneuver execution errors, and unmodeled accelerations. Moreover, safety under temporary loss of control authority is explicitly guaranteed by constraining off-nominal ballistic trajectories following a missed-thrust event (MTE) to remain outside a predefined safety region with high probability.

Two stochastic optimization strategies are compared. The first minimizes the statistical fuel cost through the ΔV_{99} metric [11, 14]. The second introduces a convex bound on nonlinear dynamical effects using higher-order dynamical information from State Transition Tensors (STTs) and semi-analytical measures of nonlinearity [16], with the objective of reducing the mismatch between linearized covariance predictions and the actual nonlinear behavior [17].

The proposed framework is demonstrated with two representative Apophis transfers between a Periodic Terminator Orbit (PTO) and a Resonant Terminator Orbit (RTO), and validated via nonlinear Monte Carlo simulations.

The paper is structured as follows: Section II defines

the model for the spacecraft dynamics, Section III formulates the optimal chance-constrained problem and outlines the solution method via sequential convex programming, Section IV showcases the numerical results. Finally, Section V summarizes the main findings of this work.

II. Dynamics modeling

This paper considers spacecraft orbital dynamics under impulsive control. Let $\boldsymbol{x} = [\boldsymbol{r}^\top, \boldsymbol{v}^\top]^\top \in \mathbb{R}^6$ and $\boldsymbol{u} \in \mathbb{R}^3$ denote the Cartesian state and control vectors, respectively, the equations of motion are modeled as a control-affine system:

$$\dot{\boldsymbol{x}} = \boldsymbol{f}_0(\boldsymbol{x}, t) + B\boldsymbol{u}(t), \quad \boldsymbol{u}(t) = \sum_{k=0}^{N-1} \boldsymbol{u}_k \, \delta(t - t_k) \tag{1}$$

where $\boldsymbol{f}_0(\cdot)$ represents the uncontrolled orbital dynamics, $B = [0_{3\times3}; \boldsymbol{I}_3]$ maps the impulsive control action into the velocity components, and $\delta(\cdot)$ denotes the Dirac delta function. The control sequence is therefore represented by a finite set of impulsive Δv maneuvers $\boldsymbol{u}_k$ applied at prescribed maneuver epochs t_k, $k = 0, \dots, N-1$ [11].

The natural dynamics $\boldsymbol{f}_0(\cdot)$ are modeled using the Augmented Normalized Hill Three-Body Problem (ANH3BP), which describes the motion of a spacecraft in the vicinity of a small body under the combined effects of the small-body gravity, solar gravity, and solar radiation pressure (SRP) [18]. In the normalized asteroid-centered Hill frame, the ANH3BP equations of motion are given by:

$$\ddot{x} = 2\dot{y} + 3x - \frac{x}{r^3} + \beta, \quad \ddot{y} = -2\dot{x} - \frac{y}{r^3} \quad \ddot{z} = -z - \frac{z}{r^3}, \tag{2}$$

where $r = \|\boldsymbol{r}\|$ and β is the nondimensional SRP parameter, measuring the relative strength of solar radiation pressure with respect to the small-body gravitational attraction [18]. The ANH3BP admits a rich set of bounded solutions and periodic orbits, including Sun-stabilized terminator orbits [18–21].

In this work, the departure and arrival science orbits are selected from the families of Periodic Terminator Orbits (PTOs) and Resonant Terminator Orbits (RTOs). PTOs are obtained by correcting frozen terminator orbit solutions into periodic orbits through differential correction and numerical continuation, following the procedures described in [19, 22]. RTOs are then identified from period-multiplying bifurcations of the PTO family, detected through the eigenvalues of the monodromy matrix, and corrected through multiple-shooting differential correction [21–23]. In particular, this paper considers transfers from a PTO to a 6:1 RTO around asteroid (99942) Apophis, selected as a representative small-body proximity-operations scenario, consistent with similar science-orbit operations planned for NASA's OSIRIS-APEX mission [24].

III. Methodology

This section summarizes the methodological framework adopted in this paper. The core architecture is illustrated in Figure 1, which outlines the safe autonomy guidance and control framework adopted in this work [11].

A chance-constrained optimal control problem is solved on the ground using sequential convex programming, incorporating models of the spacecraft dynamics, uncertainties, and mission constraints to compute safe nominal trajectories and associated linear feedback control policies. The resulting policies are validated via nonlinear Monte Carlo simulations and subsequently uploaded onboard. During flight, the spacecraft estimates its state through the onboard navigation filter and applies impulsive control actions to safely execute the transfer.

A. Original Chance-Constrained Problem Formulation

This paper formulates the science-orbit transfer under uncertainty as a stochastic optimal control problem, incorporating uncertainty arising from i) initial Gaussian state dispersion, ii) maneuver execution errors with the Gates model, iii) navigation uncertainty, and iv) unmodeled accelerations modeled as a Brownian motion, following the procedure outlined in [11, 14].

The initial state is modeled as a Gaussian random variable, while maneuver execution errors are represented as stochastic control perturbations obtained with the Gates model [25]. The navigation process is modeled as a filtering process conditioned on all past measurements, so that the control policy is based on the uncertain estimated states coming from the solution of the orbit determination (OD) problem.

To express the spacecraft dynamics, a set of nonlinear stochastic differential equations (SDEs) is adopted [11]:

$$\begin{aligned} \mathrm{d}\boldsymbol{x} &= [\boldsymbol{f}(\boldsymbol{x}, \boldsymbol{u}, t) + B\tilde{\boldsymbol{u}}\,]\,\mathrm{d}t + G(\boldsymbol{x})\mathrm{d}\boldsymbol{w}(t) \\ \boldsymbol{f}(\boldsymbol{x}, \boldsymbol{u}, t) &= \boldsymbol{f}_0(\boldsymbol{x}, t) + B\boldsymbol{u} \end{aligned} \tag{3}$$

where $\boldsymbol{f}_0(\cdot)$ denotes the natural dynamics modeled with the ANH3BP [18], $\tilde{\boldsymbol{u}}$ represents the maneuver execution error, $\mathrm{d}\boldsymbol{w}(t) \in \mathbb{R}^{n_w}$ is a standard Brownian motion, and $G(\boldsymbol{x})$ maps the Brownian motion to the dynamics of the system.

This paper models the problem in the form of a chance-constrained control problem [11–13], which aims at finding a sequence of control policies that minimize a probabilistic cost while satisfying a set of statistical constraints with a user-defined confidence level. Chance constraints are defined as [11, 26]:

$$\mathbb{P}\left[g(\boldsymbol{x}, \boldsymbol{u}, t) \leq 0\right] \geq 1 - \epsilon, \tag{4}$$

where ϵ is a user-defined risk tolerance (e.g., $\epsilon = 0.01$ for 99% confidence). This paper considers path chance constraints both in discrete and continuous-time formulations, while terminal conditions are imposed as distributional constraints, requiring the final state distribution to

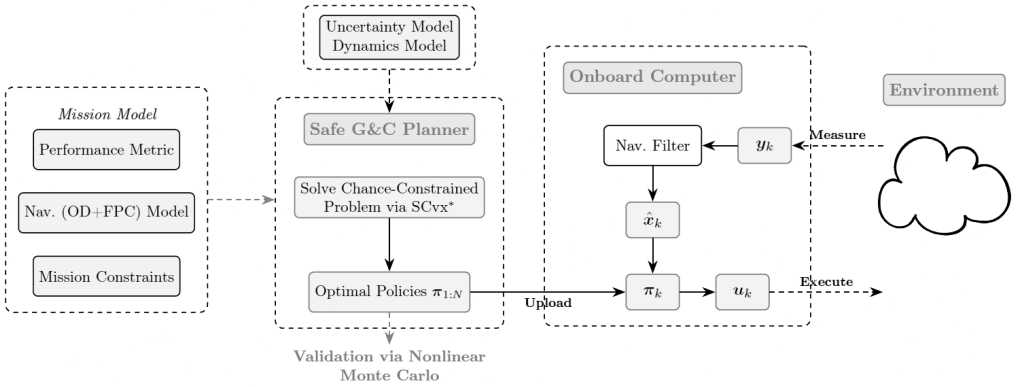

Fig. 1: Safe autonomy framework for chance-constrained guidance and control [11, 14].

match a prescribed target mean $\boldsymbol{x}_f$ and to remain below a desired terminal covariance P_f:

$$\mathbb{E}[\boldsymbol{x}_N] = \boldsymbol{x}_f, \qquad \mathrm{Cov}[\boldsymbol{x}_N] \preceq P_f \tag{5}$$

The original chance-constrained control problem can be stated as follows:

Original Chance-Constrained Problem *Find the nominal trajectory $\bar{\boldsymbol{x}}^*(t)$ and the control policies $\pi_k(\cdot)$, $\forall k = 0, \dots, N-1$ that minimize a statistical cost, subject to the nonlinear SDEs Eq. (3) and satisfying the path chance constraints Eq. (4) and terminal constraints Eq. (5), informed by the filtering process Eq. (12) of [11].*

B. Convex Reformulation via Block Cholesky Linear Covariance Steering

To solve the originally intractable stochastic problem via sequential convex programming, the nonlinear SDEs Eq. (3) are discretized into N nodes and linearized about the reference state and impulsive control $\{\boldsymbol{x}^*(t), \boldsymbol{u}^*(t)\}$ at each SCP iteration. Under the assumption of locally linear dynamics and Gaussian uncertainties, the evolution of the state distribution can be characterized entirely by its mean and covariance [11].

Following the same procedure, also the observation process Eq. (11) of [11] is linearized and a Kalman filter is used to sequentially update the state estimate. Linear covariance steering is then utilized to control both the nominal trajectory and the state distribution, while minimizing the statistical cost. The control policy $\pi_k(\cdot)$ is modeled as affine in the estimated state, as [11]:

$$\boldsymbol{u}_k = \bar{\boldsymbol{u}}_k + K_k \left(\hat{\boldsymbol{x}}_k - \bar{\boldsymbol{x}}_k \right), \tag{6}$$

where $\bar{\boldsymbol{u}}_k$ and $\bar{\boldsymbol{x}}_k$ denote the nominal control and state sequences, K_k are linear feedback gains, and $\hat{\boldsymbol{x}}_k$ is the state estimate provided by the Kalman filter.

This work uses a block-Cholesky linear covariance steering formulation to propagate the filtered state dynamics and express covariance constraints in a convex form, enabling efficient solution via SCP [11, 14].

The filtered state-estimate dynamics are written in compact block-matrix form as:

$$\hat{\boldsymbol{X}} = A\hat{\boldsymbol{x}}_0^- + B\boldsymbol{U} + C + L\tilde{\boldsymbol{Y}}, \tag{7}$$

where $\hat{\boldsymbol{X}}$ collects the estimated states, $\boldsymbol{U}$ collects the control inputs, $\tilde{\boldsymbol{Y}}$ is the innovation process, A, B, C are the linear system matrices and L contains the *a priori* calculated Kalman gains. Readers are referred to [11] for a complete derivation of the block matrices. The affine output-feedback policy is also written in block-matrix form as:

$$\boldsymbol{U} = \bar{\boldsymbol{U}} + K\boldsymbol{Z}, \qquad \boldsymbol{Z} = A\left(\hat{\boldsymbol{x}}_0^- - \bar{\boldsymbol{x}}_0\right) + L\tilde{\boldsymbol{Y}}, \tag{8}$$

where $K = \mathrm{blkdiag}(K_0, \dots, K_{N-1})$ is the feedback gain matrix and $\boldsymbol{Z}$ contains the evolution of the stochastic process given by Eq. (38) in [11]. By applying the expectation operator, it is possible to derive the nominal state and control histories, as [11]:

$$\bar{\boldsymbol{X}} = \mathbb{E}[\hat{\boldsymbol{X}}] = A\bar{\boldsymbol{x}}_0 + B\bar{\boldsymbol{U}} + C, \qquad \bar{\boldsymbol{U}} = \mathbb{E}[\boldsymbol{U}]. \tag{9}$$

where $\bar{\boldsymbol{x}}_0$ denotes the initial nominal state.

To derive the covariance matrices of the state and control evolution, let:

$$S = \mathrm{Cov}[\boldsymbol{Z}] = A\hat{P}_0^- A^\top + LP_{\tilde{Y}}L^\top, \tag{10}$$

where $\hat{P}_0^-$ is the initial state-estimate covariance and $P_{\tilde{Y}}$ is the covariance of the innovation process. Then, by applying the Cholesky factors it is possible to obtain the state-estimate and control covariances at node k, expressed as:

$$\hat{P}_k^{1/2} = E_{x_k}\left(I + BK\right)S^{1/2}, \quad P_{u_k}^{1/2} = E_{u_k}KS^{1/2}, \tag{11}$$

where E_{x_k} and E_{u_k} are extraction matrices for the state and control at node k, respectively, and $S^{1/2} = [A\hat{P}_{0^-}^{1/2} \; LP_{\tilde{Y}}^{1/2}]$. The full state covariance is then retrieved as $P_k = \hat{P}_k + \tilde{P}_k$, where $\tilde{P}_k$ is the covariance of the navigation error propagated by the Kalman filter.

In this paper, the decision variables of each convex subproblem are the nominal state and control sequences:

$$\bar{\boldsymbol{X}} = \begin{bmatrix} \bar{\boldsymbol{x}}_0^\top & \dots & \bar{\boldsymbol{x}}_N^\top \end{bmatrix}^\top, \; \bar{\boldsymbol{U}} = \begin{bmatrix} \bar{\boldsymbol{u}}_0^\top & \dots & \bar{\boldsymbol{u}}_{N-1}^\top \end{bmatrix}^\top, \quad (12)$$

together with the feedback gains $\{K_k\}_{k=0}^{N-1}$.
Since the Cholesky factors of the state and control covariance matrices are all affine functions of the optimization variables, as shown in [11], it is possible to write probabilistic constraints on the control magnitude and terminal covariance in deterministic convex form.
In particular, a maximum control magnitude chance constraint is imposed as:

$$\mathbb{P}\left[\|\boldsymbol{u}_k\|_2 \leq u_{\max}\right] \geq 1 - \epsilon_u, \quad (13)$$

and it is reformulated using the chi-square quantile as:

$$\|\bar{\boldsymbol{u}}_k\|_2 + m_{\chi^2}(\epsilon_u, n_u) \left\|P_{u_k}^{1/2}\right\|_2 \leq u_{\max}, \quad (14)$$

where P_{u_k} is the control covariance and $m_{\chi^2}(\epsilon_u, n_u)$ denotes the square root of the chi-square quantile with n_u degrees of freedom evaluated at probability $1 - \epsilon_u$.
Using the block-Cholesky formulation, the terminal constraints Eq. (5) are expressed in deterministic convex form. The terminal mean constraint becomes

$$E_{x_N}\left(A\bar{\boldsymbol{x}}_0 + B\bar{\boldsymbol{U}} + C\right) - \boldsymbol{x}_f = 0, \quad (15)$$

where E_{x_N} is a matrix defined to extract the terminal state. The terminal covariance constraint is imposed through the Cholesky factor of the terminal covariance as

$$\left\| \left(P_f - \tilde{P}_N\right)^{-1/2} E_{x_N} \left(I + BK\right) S^{1/2} \right\|_2 - 1 \leq 0, \quad (16)$$

where $\tilde{P}_N$ is the terminal estimation-error covariance propagated by the Kalman filter.

C. Continuous-Time Passive Safety Chance Constraint

This section defines the methodology adopted to enforce passive safety guarantees in the event of a loss of control authority during the autonomous science-orbit transfer, conceptually illustrated in Figure 2.
Following a missed-thrust event (MTE) at each discretization node k, the corresponding post-maneuver distribution is propagated ballistically over a safety time horizon and required to remain outside a predefined keep-out zone (KOZ) around Apophis.
The passive safety requirement is imposed as a continuous-time chance constraint on the ballistic distribution,

$$\mathbb{P}\left[\|\boldsymbol{r}(t)\|_2 \geq r_{\text{safe}}\right] \geq 1 - \epsilon_{\text{safe}}, \; \forall t \in [t_k, \, t_k + t_{\text{safety}}] \quad (17)$$

where $r_{\text{safe}} = 400$ m is the KOZ radius, ϵ_{safe} is the allowable safety-constraint violation probability, and $t_{\text{safety}} = 7$ days is the duration of the passive-safety horizon.

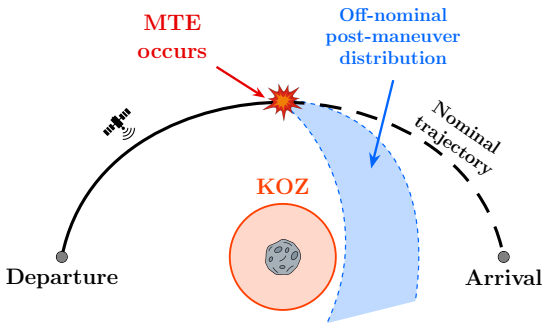

Fig. 2: Conceptual illustration of the proposed safety framework.

To prevent inter-sample violations and ensure continuous-time satisfaction of the safety requirement, a convex continuous-time chance constraint is formulated, building on the procedure outlined in [27]. First, an instantaneous penalty function is defined as:

$$\Lambda(t) \triangleq \max\Big(0, \; r_{\text{safe}} - \Big[\|\bar{\boldsymbol{r}}(t)\|_2 - m_{\chi^2}(\epsilon_{\text{safe}}, 3)\, \|P_r^{1/2}(t)\|_2\Big]\Big)^n \quad (18)$$

where $n > 1$ and ϵ_{safe} denotes the continuous-time passive safety risk bound.
Then, the spacecraft state is augmented with an auxiliary scalar variable $q(t)$ accumulating safety violations,

$$\dot{q}(t) = \Lambda(t), \; \forall t \in [t_k, \, t_k + t_{\text{safety}}] \qquad q(t_k) = 0 \quad (19)$$

Equivalently, the ballistic dynamics are augmented as

$$\dot{\boldsymbol{x}}_{\text{aug}}(t) = \begin{bmatrix} \boldsymbol{f}_0(\boldsymbol{x}(t), t) \\ \Lambda(t) \end{bmatrix}, \qquad \boldsymbol{x}_{\text{aug}}(t) = \begin{bmatrix} \boldsymbol{x}(t) \\ q(t) \end{bmatrix}. \quad (20)$$

Since $\Lambda(t) \geq 0$ by construction, enforcing:

$$q(t_k + t_{\text{safety}}) = 0, \quad \forall k \quad (21)$$

is equivalent to requiring $\int_{t_k}^{t_k + t_{\text{safety}}} \Lambda(t)\, \mathrm{d}t = 0$, which guarantees continuous-time satisfaction of the passive safety constraint over the entire safety horizon. In practice, this augmented continuous-time constraint is linearized and discretized within the SCP loop over each passive-safety propagation interval.

D. Cost Functions

Two different performance metrics are considered. The first minimizes the statistical fuel cost in terms of the 99%-quantile of the control effort by minimizing the ΔV_{99} metric:

$$J_{\Delta V_{99}} = \sum_{k=0}^{N-1} \mathcal{Q}_{\|\boldsymbol{u}_k\|_2}(p = 0.99). \quad (22)$$

Following the block-Cholesky covariance steering formulation, this cost is conservatively upper bounded in

deterministic convex form as [11, 14]:

$$J_{\Delta V_{99}} \leq \sum_{k=0}^{N-1} \left[\|\bar{\boldsymbol{u}}_k\|_2 + m_{\chi^2}(1-p, n_u) \left\| P_{u_k}^{1/2} \right\|_2 \right] \quad (23)$$

The second formulation employs the cost proposed in [17], which minimizes higher-order nonlinear errors neglected by the first-order linearization, aiming at mitigating the main limitation of linear covariance steering. The motivation is that linear covariance steering relies on locally linear dynamics and Gaussian uncertainty propagation. In highly nonlinear regimes, such as those encountered around asteroids, these assumptions inevitably break down and the actual nonlinear distribution may deviate from the distribution predicted by linear covariance analysis.

To quantify this effect, the local nonlinear propagation error is expressed from the Taylor expansion of the flow map. Let $\delta \boldsymbol{x}_k$ denote the deviation from the reference trajectory at node k. Using the Taylor series expansion (TSE) around the nominal trajectory, the propagated deviation at node $k+1$ can be written as:

$$\delta \boldsymbol{x}_{k+1} = \Phi(t_{k+1}, t_k)\, \delta \boldsymbol{x}_k + \sum_{m=2}^{\infty} \frac{1}{m!} \Phi^{(m)}(t_{k+1}, t_k)\, (\delta \boldsymbol{x}_k)^m \quad (24)$$

where $\Phi(t_{k+1}, t_k)$ is the state transition matrix (STM) and $\Phi^{(m)}(t_{k+1}, t_k)$ denotes the m-th order State Transition Tensor (STT). Standard linear covariance steering retains only the first-order STM term and neglects the higher-order remainder:

$$\mathcal{R}(\delta \boldsymbol{x}_k^+) = \sum_{m=2}^{\infty} \frac{1}{m!} \Phi^{(m)}(t_{k+1}, t_k)\, (\delta \boldsymbol{x}_k^+)^m \quad (25)$$

Let $\delta \boldsymbol{x}_k$ and $\delta \tilde{\boldsymbol{x}}_k$ denote the actual state deviation and the deviation propagated through the linearized dynamics, respectively. The nonlinear effects can be described in terms of the discrepancy between these two deviations [17]:

$$\begin{aligned} \boldsymbol{\epsilon}_1 &= \delta \boldsymbol{x}_1 - \delta \tilde{\boldsymbol{x}}_1 = \mathcal{R}_0(\delta \boldsymbol{x}_0), \\ \boldsymbol{\epsilon}_2 &= A_1 \mathcal{R}_0(\delta \boldsymbol{x}_0) + \mathcal{R}_1(\delta \boldsymbol{x}_1), \\ \boldsymbol{\epsilon}_3 &= A_2 A_1 \mathcal{R}_0(\delta \boldsymbol{x}_0) + A_2 \mathcal{R}_1(\delta \boldsymbol{x}_1) + \mathcal{R}_2(\delta \boldsymbol{x}_2). \end{aligned} \quad (26)$$

where A_k denotes the linearized dynamics from t_k to t_{k+1}. By extending this process to any future epoch t_k, it is clear that the nonlinear error $\boldsymbol{\epsilon}_k$ depends on the remainder $\mathcal{R}(\cdot)$ at the current step, as well as all the accumulated remainders from all previous steps. As a consequence, nonlinear effects progressively accumulate along the trajectory, producing a significant mismatch between the predicted linear covariance and the actual nonlinear sample distribution.

Since the exact nonlinear remainder requires the use of State Transition Tensors (STTs), it is non-convex in the optimization variables. Following the approach proposed in [17], convex upper bounds are introduced using induced tensor norms computed from the STTs [28]. The terms $\|\mathcal{A}\mathcal{R}(\delta \boldsymbol{x}_k^+)\|_2$, where $\mathcal{A} = \prod_i A_i$, are upper bounded using the triangle inequality:

$$\left\| \mathcal{A}\mathcal{R}(\delta \boldsymbol{x}_k^+) \right\|_2 \leq \sum_{m=2}^{m^*} \frac{1}{m!} g_k(\mathcal{A}, m) \left\| \delta \boldsymbol{x}_k^+ \right\|_2^m \quad (27)$$

where $g_k(\mathcal{A}, m)$ denotes the 2-norm function of the $\mathcal{B}^{(m)}$ tensor, constructed as the product between $\mathcal{A}$ and $\Phi^{(m)}(t_{k+1}, t_k)$ [17]:

$$\mathcal{B}^{(m)}_{j i_1 i_2 \ldots i_m}(t_{k+1}, t_k) = \mathcal{A}_{jk}\, \Phi^{(m)}_{k i_1 i_2 \ldots i_m}(t_{k+1}, t_k) \quad (28)$$

In this work, only the dominant second-order contribution is retained to construct a tractable measure of nonlinearity, i.e. $m^* = 2$.

Finally, it is possible to rewrite the upper bounds on the nonlinear dynamical errors in block-matrix form, obtaining Eq. (34) of [17]. The position and velocity components of this bound are then separated, yielding the quantities $\tilde{\epsilon}_{r,k}$ and $\tilde{\epsilon}_{v,k}$, which are therefore convex upper bounds of the semi-analytical nonlinear error measures. It is important to note that the STT is computed alongside the dynamics linearization process, meaning that $g_k(\cdot)$ is a constant and can be calculated *a priori* at each SCP iteration using MATLAB's Tensor Toolbox [29], reducing significantly the computational burden.

The resulting minimum nonlinearity objective is

$$J_{NL} = \max_k \left[(1-\sigma)\, \tilde{\epsilon}_{r,k} + \sigma\, \tilde{\epsilon}_{v,k} \right], \quad (29)$$

where $\sigma = 0.5$ is a scalar that balances position and velocity contributions, attributing the same weight in this work.

E. Solution Method via Sequential Convex Programming

The original non-convex stochastic optimal control problem is solved using Sequential Convex Programming. At each iteration, the problem is approximated by a convex subproblem obtained by linearizing the nonlinear dynamics and the non-convex constraints about the current reference trajectory, using a block-Cholesky formulation to express covariance propagation and chance constraints in convex form [14]. In particular, this work uses the SCvx* algorithm [30], which embeds successive convexification within an Augmented Lagrangian framework. Lagrange multipliers and a quadratic penalty are introduced for the relaxed constraints, providing theoretical guarantees of convergence to a feasible local solution of the original non-convex problem.

Starting from the deterministic reference trajectory, the stochastic problem is linearized and discretized at each iteration. To prevent *artificial unboundedness* caused by linearization, trust-region constraints are imposed on

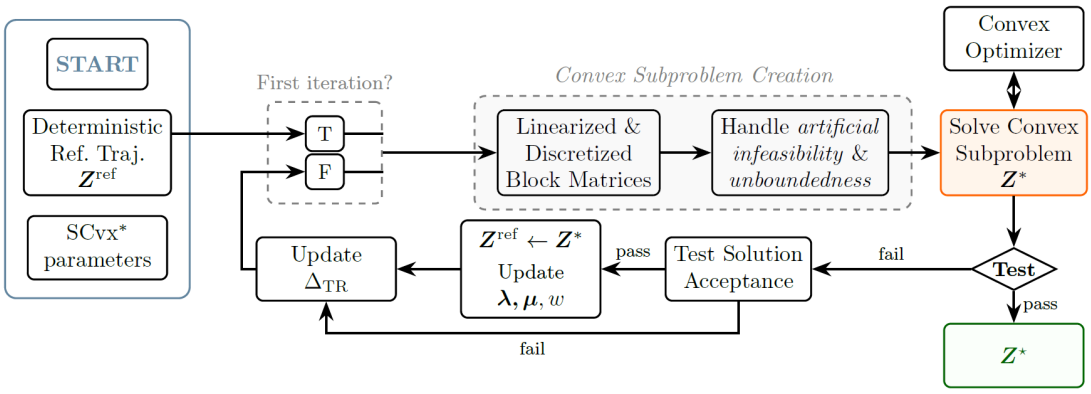

Fig. 3: Block diagram overview of algorithmic solution via SCvx*

the decision variables $\boldsymbol{Z} = \{\bar{\boldsymbol{X}}, \bar{\boldsymbol{U}}, \boldsymbol{K}\}$. To address *artificial infeasibility*, slack variables are introduced to relax the selected constraints. The cost function is augmented with penalty terms weighted by Lagrange multipliers, which penalizes constraint violations. In particular, this paper uses the 1-norm penalty introduced in [31]:

$$J_{pen}(\xi) = \boldsymbol{\lambda}^{(j)} \cdot \xi + \frac{1}{2} w^{(j)} \xi \cdot \xi + \sqrt{w^{(j)}} \|\xi\|_1 \qquad (30)$$

The resulting finite-dimensional convex subproblem is then solved to update the reference trajectory. The process is repeated until convergence in both feasibility and optimality is achieved. Figure 3 illustrates the overall iterative structure of SCvx*.

At each iteration, the convex subproblem to be solved is in the form:

$$\begin{aligned} \min_{\boldsymbol{Z}, \xi} \quad & J_{aug}(\boldsymbol{Z}, \xi) = J(\boldsymbol{Z}) + J_{pen}(\boldsymbol{\lambda}, \xi) \\ \text{s.t.} \quad & \boldsymbol{g}_{\text{eq,affine}} = 0, \quad \tilde{\boldsymbol{g}}_{\text{eq,relaxed}} = \xi \\ & \boldsymbol{h}_{\text{cvx}} \leq 0, \quad \|\boldsymbol{Z} - \boldsymbol{Z}^{\text{ref}}\|_\infty \leq \Delta_{\text{TR}}, \end{aligned}$$

Here, $\boldsymbol{g}_{\text{eq,affine}} = 0$ includes the linearized filtered state dynamics and control constraints Eq. (9), $\boldsymbol{h}_{\text{cvx}} \leq 0$ represents the control magnitude constraint Eq. (14) and convex terminal covariance constraint Eq. (16), while $\tilde{\boldsymbol{g}}_{\text{eq,relaxed}}$ collects the relaxed terminal mean Eq. (15) and continuous-time passive safety constraints Eq. (21).

IV. Numerical Results

This section presents the numerical results obtained by applying the previously introduced framework to two PTO-RTO transfers around Apophis. The solutions are validated through nonlinear Monte Carlo simulations ($N_{\text{MC}} = 500$ samples) by propagating the full nonlinear SDEs under the optimized control policies, following the procedure proposed in [14].

To initialize the stochastic optimization, a deterministic reference trajectory is first generated using an Adaptive-Mesh sequential convex programming (AMSCP) framework [32], which directly optimizes both impulsive maneuvers and the time discretization. This approach places the control actions at optimal epochs, approaching as closely as possible the theoretical optimum provided by Pontryagin's Minimum Principle while retaining numerical efficiency. The method enables the generation of free-phase optimal trajectories from the departing PTO to the arrival 6:1 RTO with bounded time of flight, optimizing the departure and arrival locations as well as the transfer duration.

The convex subproblems are modeled in MATLAB using YALMIP and solved with MOSEK.

A. Multiple Revolution Transfer

The first case study involves a multi-revolution transfer. The robust nominal trajectories for both optimization strategies are showcased in Figure 4.

Although the nominal trajectories are geometrically similar, the two solutions differ significantly in their control structure, particularly in the trajectory correction maneuver (TCM) policies, as shown in Figure 5. The minimum ΔV_{99} formulation primarily relies on nominal feedforward maneuvers, with limited feedback TCMs to reduce the statistical fuel cost. In contrast, the minimum nonlinear error solution introduces more aggressive TCMs to actively control the dispersion and maintain it within the locally linear and Gaussian regime.

As a consequence, in the minimum ΔV_{99} case the nonlinear MC samples progressively deviate from the linear prediction, leading to a terminal distribution that does not fully satisfy the target statistics, as shown in Figure 6. This discrepancy is the result of the accumulation of nonlinear effects in the ANH3BP dynamics, and the real distribution quickly becomes non-Gaussian. Conversely, the minimum nonlinear error mitigates these effects, resulting in a much closer agreement between the predicted and sample terminal distributions.

This improved consistency is achieved at the expense of a slightly higher fuel cost, although its increase remains limited to a few mm/s, as shown in Table 1.

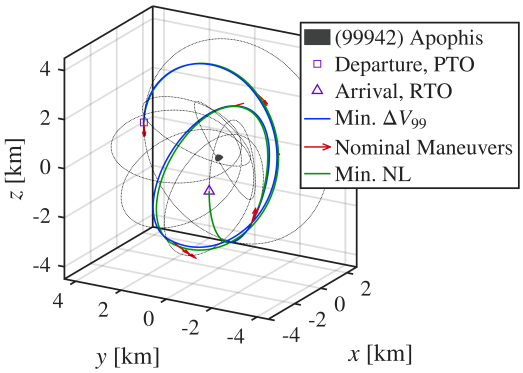

Fig. 4: Robust nominal trajectories (Case Study 1).

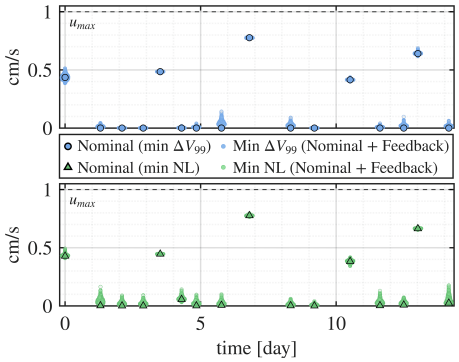

Fig. 5: MC control magnitudes at discrete maneuver epochs for Min. ΔV_{99} and Min. NL strategies (Case Study 1).

B. *Fly-by Transfer*

The second case study considers a flyby transfer with a close approach to Apophis.

The robust nominal trajectories are showcased in Figure 7. In this case, the minimum ΔV_{99} strategy results in a higher and more conservative nominal flyby altitude, due to the safety constraints and the larger dispersions associated with its solution. In contrast, the minimum nonlinear error solution allows a closer nominal approach.

The nonlinear Monte Carlo results for the nominal operations exhibit trends similar to Case Study 1 and are omitted for brevity. Figure 8 shows the comparison between the Monte Carlo trajectories obtained in open loop (i.e., with $K_k = 0 \ \forall k$) and in closed loop for the minimum nonlinear error solution, highlighting the essential role of TCMs for robust autonomous science-orbit transfers under uncertainty. In the open loop case, the dispersion grows significantly along the transfer, leading to large deviations from the nominal trajectory, while the closed loop simulation shows active regulation of the dispersion through the feedback controls, maintaining the distribution within the locally linear regime and ensuring convergence toward the target distribution.

In this case study, greater insight is obtained by analyzing off-nominal scenarios, where MTEs are simulated at each maneuver epoch. A separate off-nominal Monte Carlo analysis is performed and the resulting ballistic trajectories, propagated from each node over the full safety horizon, are shown in Figure 9. Both strategies are effective in guaranteeing passive safety, with only minimal KOZ violations exhibited by the minimum nonlinear error solution.

Although the minimum nonlinear error solution starts from smaller post-maneuver covariances, the resulting ballistic dispersion appears larger in the MTE simula-

Table 1. Monte Carlo ΔV statistics for minimum ΔV_{99} and minimum nonlinear error objectives (Case Study 1).

	Min. ΔV_{99}	**Min. NL**
Nominal ΔV [cm/s]	2.75	2.80
Mean MC ΔV [cm/s]	2.91	3.06
MC ΔV_{99} [cm/s]	3.17	3.41

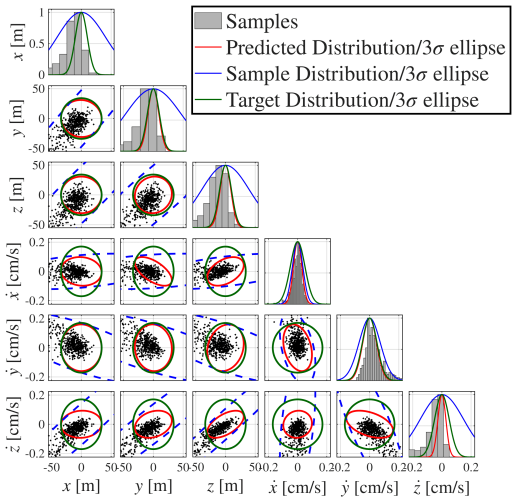

(a) With minimum ΔV_{99}

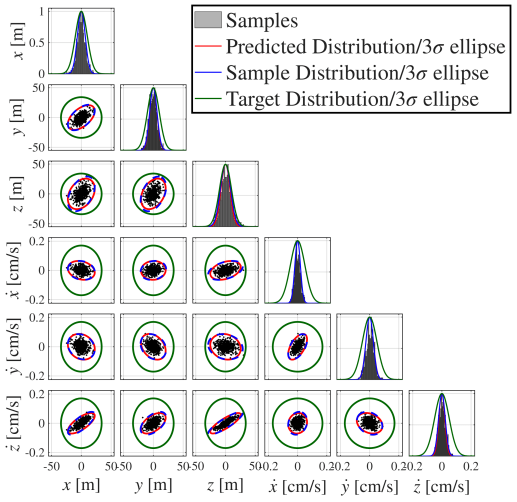

(b) With minimum nonlinear error

Fig. 6: State distribution at target node (Case Study 1).

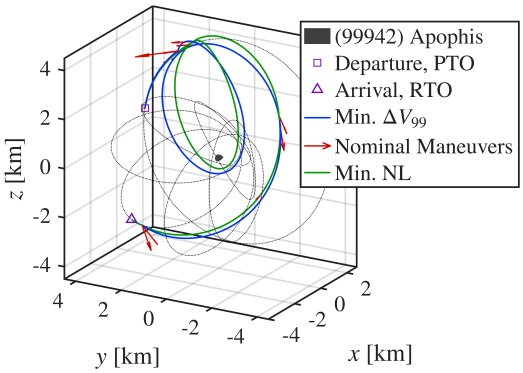

Fig. 7: Robust nominal trajectories (Case Study 2).

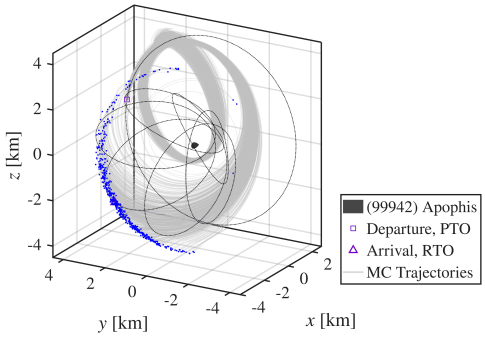

(a) Open Loop (i.e., $K_k = 0\ \forall k$).

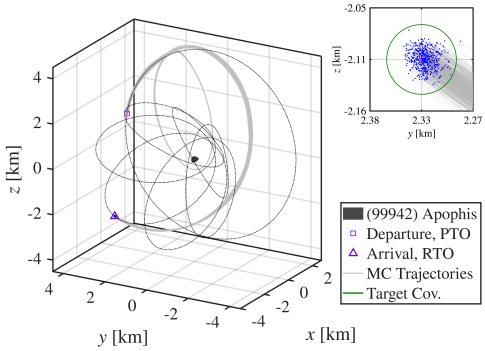

(b) Closed Loop (Min. NL).

Fig. 8: Open vs Closed Loop MC Trajectories (Case Study 2).

tions. This is not due to higher uncertainty levels, but to the structure of the control profile. The minimum ΔV_{99} trajectory contains several nearly ballistic segments with limited corrective action, so MTEs at those nodes have minor impact and the overall deviations remain more contained. This indicates that robustness to missed-thrust events depends not only on covariance magnitude, but also on the frequency of control actions. To this end, introducing sparsity-promoting techniques [33, 34] within the minimum nonlinear error framework to reduce TCMs could provide a more favorable trade-off between terminal distribution robustness and passive safety under MTE scenarios.

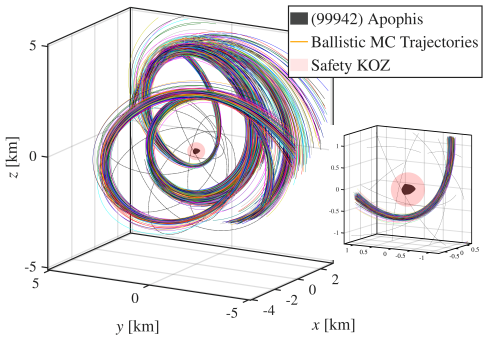

(a) With minimum ΔV_{99}

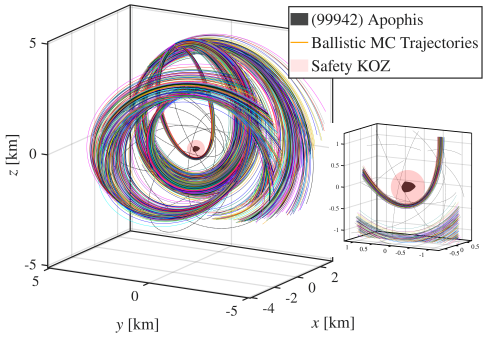

(b) With minimum nonlinear error

Fig. 9: Ballistic trajectories after MTEs (Case Study 2).

V. Conclusions

A chance-constrained covariance steering framework is applied to safe autonomous science-orbit transfers around small bodies. The proposed formulation jointly designs nominal impulsive trajectories and feedback trajectory correction policies while enforcing terminal distribution constraints and continuous-time passive safety guarantees against missed-thrust events. Numerical results for PTO–RTO transfers around Apophis show that both tested objectives can successfully provide probabilistic passive safety in case of loss of control authority. Minimizing the ΔV_{99} metric results in solutions with limited corrective feedback and reduced control effort, but the accumulation of nonlinear effects leads to significant discrepancies between the predicted and actual state distributions. In contrast, minimizing the nonlinear errors results in improved consistency between linear covariance predictions and nonlinear Monte Carlo samples, at the cost of a marginal increase in fuel consumption.

APPENDIX

A. Uncertainty parameters

The uncertainty parameters used in the numerical simulations are summarized in Table 2. The initial state distribution is modeled as $P_0 = \hat{P}_0^- + \tilde{P}_0^-$, where the prior state-estimate covariance is defined as $\hat{P}_0^- = \text{blkdiag}(\sigma_{r,0}^2 I_3, \sigma_{v,0}^2 I_3)$ and the initial estimation-error covariance is $\tilde{P}_0^- = \text{blkdiag}((\sigma_r^{\text{nav}})^2 I_3, (\sigma_v^{\text{nav}})^2 I_3)$. The target terminal distribution is defined as $P_f = \text{blkdiag}(\sigma_{r,f}^2 I_3, \sigma_{v,f}^2 I_3)$. For the minimum-$\Delta V_{99}$ formulation, a maximum covariance bound $P_{\max} = \text{blkdiag}(\sigma_{r,\max}^2 I_3, \sigma_{v,\max}^2 I_3)$ is additionally imposed to limit uncertainty growth and preserve the validity of the local linear-Gaussian approximation. Maneuver execution errors are modeled through the Gates model, parameterized by fixed and proportional magnitude errors, σ_1 and σ_2, and fixed and proportional pointing errors, σ_3 and σ_4. The navigation process is approximated as a full-state observation with Gaussian noise, i.e., $f_{\text{obs}}(\boldsymbol{x}_k) = \boldsymbol{x}_k$ and $G_{\text{obs}} = \text{blkdiag}(\sigma_r^{\text{nav}} I_3, \sigma_v^{\text{nav}} I_3)$. Unmodeled accelerations are represented as a stochastic acceleration acting only on the velocity dynamics, with diffusion matrix $G = [0_{3\times3}, \sigma_{\text{stoch}}\sqrt{\Delta t}\, I_3]^\top$ after time discretization. Finally, the control magnitude and chance constraints are enforced with risk parameters ϵ_u and ϵ_{safe}, respectively.

B. SCvx* parameters

The SCvx* parameters adopted in the stochastic optimization are briefly reported in this section. The feasibility tolerance is set to $\epsilon_{\text{feas}} = 10^{-6}$, while the optimality tolerance ϵ_{opt} is selected depending on the objective function: a value of 10^{-6} is used for the minimum-ΔV_{99} formulation, while 10^{-4} is selected for the minimum-nonlinearity formulation due to the higher computational cost and numerical complexity. The step acceptance and trust-region parameters $\{\eta_0, \eta_1, \eta_2\}$ and $\{\alpha_1, \alpha_2\}$ are selected as those in [14], as well as the augmented Lagrangian parameters β, γ, $w^{(1)}$ and $w_{\max}$. The trust-region radius is initialized at $\Delta^{(1)} = 0.2$ and constrained between $\Delta_{\min} = 10^{-8}$ and $\Delta_{\max} = 1$.

Table 2. Uncertainty and constraint parameters

Quantity	Symbol	Value	Unit
initial dispersion (pos.)	$\sigma_{r,0}$	25	m
initial dispersion (vel.)	$\sigma_{v,0}$	0.5	mm/s
initial est. error (pos.)	σ_r^{nav}	0.5	m
initial est. error (vel.)	σ_v^{nav}	0.1	mm/s
terminal dispersion (pos.)	$\sigma_{r,f}$	10	m
terminal dispersion (vel.)	$\sigma_{v,f}$	0.5	mm/s
max. cov. bound (pos.)	$\sigma_{r,\max}$	150	m
max. cov. bound (vel.)	$\sigma_{v,\max}$	2.5	mm/s
exec. error (fixed mag.)	σ_1	10^{-2}	mm/s
exec. error (prop. mag.)	σ_2	0.33	%
exec. error (fixed point.)	σ_3	10^{-2}	mm/s
exec. error (prop. point.)	σ_4	0.2	deg
stochastic acceleration	σ_{stoch}	10^{-13}	km/s^2
max. ΔV magnitude	$u_{\max}$	1.5	cm/s
risk bound (control)	ϵ_u	10^{-3}	–
risk bound (safety)	ϵ_{safe}	10^{-2}	–

REFERENCES

[1] DJ Scheeres and JW McMahon. Autonomous Architectures for Small Body Exploration. In *2019 AAS/AIAA Astrodynamics Specialist Conference*, 2019.

[2] Shota Takahashi and Daniel J Scheeres. Autonomous Exploration of a Small Near-Earth Asteroid. *Journal of Guidance, Control, and Dynamics*, 44(4):701–718, 2021.

[3] Issa AD Nesnas, Benjamin J Hockman, Saptarshi Bandopadhyay, Benjamin J Morrell, Daniel P Lubey, Jacopo Villa, David S Bayard, Alan Osmundson, Benjamin Jarvis, Michele Bersani, et al. Autonomous Exploration of Small Bodies Toward Greater Autonomy for Deep Space Missions. *Frontiers in Robotics and AI*, 8:650885, 2021.

[4] Roberto Furfaro. Hovering in Asteroid Dynamical Environments Using Higher-Order Sliding Control. *Journal of Guidance, Control, and Dynamics*, 38(2):263–279, 2015.

[5] Rodolfo Batista Negri, Antônio FBA Prado, Ronan AJ Chagas, and Rodolpho V Moraes. Autonomous Rapid Exploration in Close-Proximity of Asteroids. *Journal of Guidance, Control, and Dynamics*, 47(5):914–933, 2024.

[6] Claudio Bottiglieri, Felice Piccolo, Carmine Giordano, Fabio Ferrari, and Francesco Topputo. Applied Trajectory Design for CubeSat Close-Proximity Operations around Asteroids: The Milani Case. *Aerospace*, 10(5):464, 2023.

[7] Erica L Jenson and Daniel J Scheeres. Multi-Objective Optimization of Covariance and Energy for Asteroid Transfers. *Journal of Guidance, Control, and Dynamics*, 44(7):1253–1265, 2021.

[8] Kenshiro Oguri and Jay W McMahon. Robust Spacecraft Guidance around Small Bodies under Uncertainty: Stochastic Optimal Control Approach. *Journal of Guidance, Control, and Dynamics*, 44(7):1295–1313, 2021.

[9] Kenshiro Oguri and Jay W McMahon. Stochastic Primer Vector for Robust Low-Thrust Trajectory Design Under Uncertainty. *Journal of Guidance, Control, and Dynamics*, 45(1):84–102, 2022.

[10] Antonio Rizza, Simone D'Amico, and Francesco Topputo. Goal-Oriented Trajectory Refinement for Asteroid Mapping Using Sequential Convex Programming. *Journal of Guidance, Control, and Dynamics*, 48(11):2447–2461, 2025.

[11] K. Oguri. Chance-Constrained Control for Safe Spacecraft Autonomy: Convex Programming Approach. In *2024 IEEE American Control Conference*, 2024.

[12] Kazuhide Okamoto, Maxim Goldshtein, and Panagiotis Tsiotras. Optimal Covariance Control for Stochastic Systems Under Chance Constraints. *IEEE Control Systems Letters*, 2(2):266–271, 2018.

[13] Jack Ridderhof, Kazuhide Okamoto, and Panagiotis Tsiotras. Chance Constrained Covariance Control for Linear Stochastic Systems with Output Feedback. In *2020 59th IEEE Conference on Decision and Control (CDC)*, pages 1758–1763. IEEE, 2020.

[14] Kenshiro Oguri and Gregory Lantoine. Convex Block-Cholesky Approach to Risk-Constrained Low-thrust Trajectory Design under Operational Uncertainty. *arXiv preprint arXiv: 2602.18416*, 2026.

[15] Naoya Kumagai and Kenshiro Oguri. Robust Cislunar Low-Thrust Trajectory Optimization Under Uncertainties via Sequential Covariance Steering. *Journal of Guidance, Control, and Dynamics*, 48(12):2725–2743, 2025.

[16] Erica L Jenson and Daniel J Scheeres. Semianalytical Measures of Nonlinearity based on Tensor Eigenpairs. *Journal of Guidance, Control, and Dynamics*, 46(4):638–653, 2023.

[17] Daniel C. Qi and Kenshiro Oguri. Convex Bound of Nonlinear Dynamical Errors for Covariance Steering. *Journal of Guidance, Control, and Dynamics*, 2026. In press.

[18] DJ Scheeres and Francesco Marzari. Spacecraft Dynamics in the Vicinity of a Comet. *The Journal of the astronautical sciences*, 50(1):35–52, 2002.

[19] Daniel J. Scheeres. *Orbital Motion in Strongly Perturbed Environments: Applications to Asteroid, Comet and Planetary Satellite Orbiters*. Springer Berlin, Heidelberg, 2012.

[20] Stephen B Broschart and Benjamin F Villac. Identification of Non-Chaotic Terminator Orbits Near 6489 Golevka. *Advances in the Astronautical Sciences*, 134:861–880, 2009.

[21] Stephen B Broschart, Daniel J Scheeres, and Benjamin F Villac. New Families of Multi-Revolution Terminator Orbits Near Small Bodies. *Advances in the Astronautical Sciences*, 135(3):1685–1702, 2009.

[22] Stephen B. Broschart, Gregory Lantoine, and Daniel J. Grebow. Quasi-Terminator Orbits Near Primitive Bodies. *Celestial Mechanics and Dynamical Astronomy*, 120(2):195–215, October 2014.

[23] Zimovan Spreen. *Trajectory Design And Targeting Applications to the Exploration Program in Cislunar Space*. Ph.d. dissertation, Purdue University, 2021.

[24] Daniella N DellaGiustina, Michael C Nolan, Anjani T Polit, Michael C Moreau, Dathon R Golish, Amy A Simon, Coralie D Adam, Peter G Antreasian, Ronald-Louis Ballouz, Olivier S Barnouin, et al. OSIRIS-APEX: an OSIRIS-REx Extended Mission to Asteroid Apophis. *The Planetary Science Journal*, 4(10):198, 2023.

[25] Clarence R Gates. A Simplified Model of Midcourse Maneuver Execution Errors. Technical report, Jet Propulsion Laboratory, California Institute of Technology (Report No. 32-504), 1963.

[26] Boris Benedikter, Alessandro Zavoli, Zhenbo Wang, Simone Pizzurro, and Enrico Cavallini. Convex Approach to Covariance Control with Application to Stochastic Low-Thrust Trajectory Optimization. *Journal of Guidance, Control, and Dynamics*, 45(11):2061–2075, 2022.

[27] Purnanand Elango, Dayou Luo, Abhinav G Kamath, Samet Uzun, Taewan Kim, and Behçet Açıkmeşe. Successive Convexification for Trajectory Optimization with Continuous-Time Constraint Satisfaction. *arXiv preprint arXiv:2404.16826*, 2024.

[28] Jackson Kulik, Maximilian Ruth, Cedric Orton-Urbina, and Dmitry Savransky. Applications of Induced Tensor Norms to Guidance Navigation and Control. *Journal of Guidance, Control, and Dynamics*, 48(10):2180–2198, 2025.

[29] Kolda Tamara G. Bader, Brett W. et al. Tensor Toolbox for MATLAB, Version 3.8, 2025.

[30] Kenshiro Oguri. Successive Convexification with Feasibility Guarantee via Augmented Lagrangian for Non-Convex Optimal Control Problems. In *2023 62nd IEEE Conference on Decision and Control (CDC)*, pages 3296–3302. IEEE, 2023.

[31] Kenshiro Oguri and Gregory Lantoine. Lossless Control-Convex Formulation for Solar-Sail Trajectory Optimization via Sequential Convex Programming. *Journal of Guidance, Control, and Dynamics*, 48(2):311–326, 2025.

[32] Naoya Kumagai and Kenshiro Oguri. Adaptive-Mesh Sequential Convex Programming for Space Trajectory Optimization. *Journal of Guidance, Control, and Dynamics*, 47(10):2213–2220, 2024.

[33] Naoya Kumagai and Kenshiro Oguri. Hands-Off Covariance Steering: Inducing Feedback Sparsity via Iteratively Reweighted l1,p Regularization. In *2025 IEEE 64th Conference on Decision and Control (CDC)*, pages 3560–3565. IEEE, 2025.

[34] G. Nuccio, K. Oguri, and F. Topputo. Statistical Trajectory Optimization Under Uncertainty for Icy Moon Exploration with Probability of Impact Constraints. In *30th International Symposium on Space Flight Dynamics (ISSFD)*, 2026.